Ab initio study of Cr interactions with point defects in bcc Fe

Pär Olsson,[1,2] Christophe Domain,[1] and Janne Wallenius[2,3]
[1]*Department Matériaux et Mécanique des Composants, EDF-R&D, Les Renardières, F-77250 Moret sur Loing, France*
[2]*Department of Neutron Research, Uppsala University, Uppsala, Sweden*
[3]*Department of Nuclear and Reactor Physics, Royal Institute of Technology, Stockholm, Sweden*
(Received 23 August 2005; revised manuscript received 13 October 2006; published 19 January 2007)

The properties of Cr in α Fe have been investigated by *ab initio* calculations based on density functional theory. The intrinsic point defect formation energies were found to be larger in model bcc Cr as compared to those in ferromagnetic bcc Fe. The interactions of Cr with point defects (vacancy and self-interstitials) have been characterized. Single Cr atoms interact weakly with vacancies but significantly with self-interstitial atoms (SIA). Mixed interstitials of any interstitial symmetry are bound. Configurations where two Cr atoms are in nearest-neighbor position are generally unfavorable in bcc Fe except when they are a part of a $\langle 111 \rangle$ interstitial complex. Mixed $\langle 110 \rangle$ interstitials do not have as strong directional stability as pure Fe interstitials have. The effects on the results using the atom description scheme of either the ultrasoft pseudopotential (USPP) or the projector augmented wave (PAW) formalisms are connected to the differences in local magnetic moments that the two methods predict. As expected for the Fe-Cr system, the results obtained using the PAW method are more reliable than the ones obtained with USPP.

DOI: 10.1103/PhysRevB.75.014110 PACS number(s): 61.72.Ji, 71.15.Mb, 71.20.Be

I. INTRODUCTION

The development of new reactors as well as the maintenance of in service reactors require a good understanding of the behavior of the structural material under irradiation. Neutron and proton irradiation of the materials lead to hardening and embrittlement that strongly depend on the chemical composition. Ferritic martensitic steels can be good structural materials for fast neutron reactors, and in particular high-Cr reduced-activation steels.[1–3] In Fe-Cr alloys, Cr plays a major role in the radiation-induced evolution of the mechanical properties. A content of 2 to 6 % Cr reduces the swelling compared to pure Fe,[1,3] whereas the optimal Cr content regarding the brittle ductile transition is 9%.[4] In addition, under neutron irradiation the interstitial loops formed have different characteristics depending on the Cr content. For low Cr concentrations (2% to 6% Cr) the loops have the $a\langle 100 \rangle$ Burgers vector, whereas a mixed population with $a\langle 100 \rangle$ and $a/2\langle 111 \rangle$ Burgers vectors have been observed for high-Cr content Fe-Cr alloys (12% and 18% Cr).[5]

In order to understand the mechanical properties of Fe-Cr alloys under irradiation, knowledge about the interactions of Cr with the various defects that are formed (defect clusters, dislocation loops) and with point defects is of great importance. Understanding of the impact on the kinetic evolution of the microstructure of the material can be provided from atomistic simulations where useful information on the elementary interactions and mechanisms can be obtained.

Atomistic simulations using molecular dynamics with empirical potentials have previously been performed by Konishi *et al.*[6] They constructed a Finnis Sinclair Fe-Cr potential which predicted 0.12 eV binding between the self-interstitial (SIA) and a nearby Cr, but the most stable configuration for the self-interstitial was the $\langle 111 \rangle$Fe crowdion, in disagreement with recent *ab initio* calculations.[7,8]

Cascades have been simulated[9] and the diffusion in Fe-Cr alloys by vacancy and interstitial mechanisms has been studied.[10] These simulations are based on embedded atom method (EAM) potentials which were fitted mainly on lattice parameters, elastic constants and mixing enthalpies.[11] In order to better reproduce the point defect interactions in Fe-Cr with an empirical potential, it should be fitted explicitly to *ab initio* calculations of defect interactions. Recently, an Fe potential,[12] an Fe-P potential,[13] and an Fe-Cr potential[14] has been successfully fitted in this way. In the Fe-Cr potential, the EAM scheme has been enriched by an additional term in order to reproduce the nonmonotonic variation of the mixing enthalpy,[15] and to allow simulations of the formation of the α' phase during thermal aging of the Fe-Cr alloy.[14] These recent works emphasize the importance of the use of defect configuration energies to build more accurate empirical potentials. Explicit knowledge about the character of the point defect interactions with solute Cr in bcc Fe will be important for the multiscale modeling of the time evolution of the microstructure under aging and in particular under irradiation.

The objective of this work is to determine and discuss in detail some properties of the Fe-Cr system using density functional theory calculations. The determination of the interactions of Cr in solid solution in bcc Fe with point defects such as vacancies and interstitials depend strongly on the chemical interactions since Cr and Fe have similar atomic sizes.

After describing the *ab initio* method used, the properties of the intrinsic point defects in bcc Fe and bcc Cr are presented. Then the mixing enthalpy of the Fe-Cr system is shown. The interactions of one and two Cr atoms with a vacancy as well as with the different self-interstitial configurations will be exposed and the consequences of these findings will be discussed. Finally, the effect of magnetism on the different configurations is discussed.

II. METHODOLOGY

Ab initio calculations have been performed within density functional theory (DFT), using pseudopotentials generated within the projector augmented wave (PAW) approach[16,17] and with ultrasoft pseudopotentials (USPP)[16–19] implemented in the Vienna *ab initio* simulation package (VASP).[20–22] The USPP formalism can be derived from the PAW formalism by linearization. In general, the USPP method does not describe transition metals and magnetic systems as well as the PAW method does and is included as a point of reference in order to show the importance of using as correct methods as possible.[23] The pseudopotentials were from the VASP library. The calculations were spin polarized and the exchange-correlation functional used is the generalized gradient approximation (GGA) of Perdew and Wang[24] with the Vosko-Wilk-Nusair (VWN) interpolation of the correlation energy.[25] While it is not crucial to use the VWN interpolation when it comes to the prediction of properties in most pure metals, it is however important when studying ferromagnetic alloys as the delicate interchemical interactions are strongly coupled with the local magnetizations.

Periodic boundary conditions and the supercell approach was used for all calculations. Brillouin zone sampling was performed using the Monkhorst and Pack scheme.[26] The electronic configurations of Fe and Cr are Ar $3d^7 4s^1$ and Ar $3d^5 4s^1$, respectively. The defect calculations are performed at constant volume, relaxing the atomic position using the conjugate gradient algorithm. The equilibrium lattice parameter for bcc Fe has been used if not otherwise mentioned. The energies calculated are converged with 125 k points sampling for 54 atom supercells and 27 k points with 128 atom supercells, following the convergence tests explained in a previous work.[7] The plane wave cutoff energy used with PAW is 300 eV and 240 eV with USPP.

The local magnetic moments are defined as the difference in spin channel occupation after projection on spheres with the Wigner-Seitz radii suggested in the pseudopotential data files. For Fe it is 1.30 Å and for Cr 1.32 Å.

The mixing energy is defined as the deviation in energy for a given alloy composition from the linear combination of the energy of the pure elements. For an alloy composition of x parts Fe and $(1-x)$ parts Cr it is

$$E_{\mathrm{mix}}(\mathrm{Fe}_x\mathrm{Cr}_{1-x}) = E(\mathrm{Fe}_x\mathrm{Cr}_{1-x}) - \{xE[\mathrm{Fe}] + (1-x)E[\mathrm{Cr}]\}, \tag{2.1}$$

where $E[\mathrm{Fe}]$ is the energy per atom of the bcc Fe supercell with the same size, and $E[\mathrm{Cr}]$ is the energy per atom of nonmagnetic (NM) bcc Cr.

The formation energy of a configuration containing N sites with n Fe atoms and p Cr atoms is defined as

$$E_{\mathrm{for}}(n\mathrm{Fe} + p\mathrm{Cr}) = E[n\mathrm{Fe} + p\mathrm{Cr}] - nE[\mathrm{Fe}] - pE[\mathrm{Cr}]. \tag{2.2}$$

The total binding energy between n objects, i.e., vacancies, self-interstitial atoms, or Cr atoms, is the energy difference between the configuration where all the objects interact, and the system where all the objects are far from each other in order not to interact. Due to the limited supercell size and in order to subtract supercell energies obtained with the same cutoff and k points mesh, the total binding energy is calculated as

$$E_{\mathrm{b}}(A_1, A_2, \ldots, A_n) = \sum_{i=1,n} E(A_i) - [E(A_1 + A_2 + \cdots + A_n) + (n-1)E_{\mathrm{ref}}], \tag{2.3}$$

where E_{ref} is the energy of the supercell without any defects A_i, $E(A_i)$ is the energy of the supercell with A_i, and $E(A_1+A_2+\cdots+A_n)$ is the energy of the cell containing all A_i interacting defects. All the supercells contain the same number of sites, i.e., have the same size.

TABLE I. Lattice parameter in Å for ferromagnetic (FM) bcc Fe, nonmagnetic (NM), and antiferromagnetic (AF) bcc Cr.

Structure	PAW	USPP	Expt.[a]
Fe bcc FM	2.831	2.879	2.86
Cr bcc NM	2.836	2.851	—
Cr bcc AF	2.850	2.918	2.88

[a]Reference 30.

III. RESULTS

A. Equilibrium structures

For bcc Fe, the reference state is the ferromagnetic phase. Whereas for bcc Cr, the magnetic state is much more complicated,[27–29] and different "extreme" cases which are nonmagnetic and antiferromagnetic have been considered.

The lattice parameters obtained for pure Fe and Cr are shown in Table I. Compared to the measured lattice parameters, the calculated values are smaller by up to 1%. The difference between the lattice parameters of Fe and Cr (0.02 Å) is better reproduced using PAW. Cr is larger than Fe only using PAW. For USPP, only the antiferromagnetic Cr is larger than Fe. The absolute discrepancy remains small in all cases, and should not affect results regarding point defect interactions, for which chemical effects will have a larger contribution. The calculated equilibrium parameters are used hereafter for constant volume calculations with 54 and 128 atom supercells using the method stated above.

For Fe, the local magnetic moment with PAW ($\mu_{\mathrm{PAW}} = 2.21\mu_{\mathrm{B}}$) is closer to the experimental value of $2.22\mu_{\mathrm{B}}$ (Ref. 30) than the one predicted by USPP ($\mu_{\mathrm{USPP}} = 2.52\mu_{\mathrm{B}}$) is. This difference seems to be an intrinsic feature of the formalisms, and does not originate directly from the difference in lattice parameters. PAW calculations using the USPP lattice parameter changes the local magnetic moment by only $0.08\mu_{\mathrm{B}}$.

For Cr in the antiferromagnetic state, the local magnetic moment per Cr atom is $\pm 0.92\mu_{\mathrm{B}}$ using PAW and $\pm 1.97\mu_{\mathrm{B}}$ using USPP. The differences in predicted magnetization are the first indications of a substantial difference between the two formalisms. The USPP for Cr allows for a much larger relaxation of the magnetic moments than PAW does and

TABLE II. Point defect formation energy (eV) in pure bcc Fe. PAW and USPP calculations with 54 atom supercells and 125 k points and 128 atom supercells and 27 k points.

Defect	54 at. PAW	128 at. PAW	Fu *et al.*[a]	54 at. USPP	128 at. USPP
Vacancy	2.12	2.15	2.07	1.93	2.02
⟨100⟩	5.36	5.13	4.64	5.07	5.04
⟨110⟩	4.13	4.02	3.64	3.96	3.94
⟨111⟩	4.89	4.72	4.34	4.75	4.66
Octahedral	5.51	5.29	4.94	5.35	5.25
Tetrahedral	4.56	4.44	4.26	4.53	4.46

[a]Reference 8.

overestimates the antiferromagnetic interaction. The PAW result is in better agreement with the measured $0.7\mu_B$ magnetic moment amplitude of the spin density wave state in Cr.[31]

B. Intrinsic point defects in bcc Fe

The intrinsic point defect formation energies reported in Table II are similar for PAW and USPP. The vacancy formation energy is about 2.1 eV using PAW and 0.1 eV lower using USPP. As already discussed,[7] for self-interstitials, the most stable interstitial configuration is the ⟨110⟩ dumbbell. The calculated energy difference between the ⟨110⟩ and ⟨111⟩ configurations is 0.7 eV using both formalisms. Furthermore, the tetrahedral configuration is more stable than the ⟨111⟩ crowdion. These results are in agreement with the *ab initio* calculations of Fu *et al.*[8] based on numerical orbitals with relaxation under constant pressure using 128-atom supercells. One can notice that the different strategies to relax the system, i.e., considering constant volume or relaxed volume (with a zero pressure condition) does not significantly affect the results.

The effect of the supercell size, comparing 54- and 128-atom supercells, is rather small. For a vacancy the difference is on the order of 10 meV, whereas for self-interstitials, due to the larger distortion induced by the interstitial defect, the energy difference is on the order of 100 meV.

Regarding the influence of the presence of point defects on the local magnetic moments on the Fe atoms, the results obtained using PAW are similar to the ones using USPP in a previous work by Domain and Becquart.[7] For the vacancy (Table III), the magnetic moments of the Fe atoms in first nearest-neighbor position is increased, as would be expected from the larger volume in which to relax the moments. For self-interstitials, the local magnetic moment of the two Fe atoms within the interstitial is small and the moment on the nearest-neighbor atoms is reduced in the compression positions whereas it is enhanced in the tensile positions [Figs. 1(a), 1(b), 2(a), and 2(b)].

In most cases the changes in the local magnetic moments with respect to those of the perfect crystal are similar using PAW or USPP. For instance, for the ⟨110⟩ configuration, the relative variations of the moments of the nearest-neighbor Fe atoms are independent of formalism, as well as for the two atoms within the dumbbell (Fig. 1). For the ⟨111⟩ configuration (Fig. 2), the two atoms within the interstitial have an antiferromagnetic (AF) spin ($-0.5\mu_B$) using PAW and a small ferromagnetic spin ($0.3\mu_B$) using USPP. In addition, probably due to magnetic coupling, the magnetic moment on the first nearest Fe atoms is larger using PAW ($1.53\mu_B$) than for USPP ($1.16\mu_B$). Even though the description of local magnetism in defects only differ significantly in the case of the ⟨111⟩ interstitial, this apparently does not affect the formation energies, as the directional stability is identical for both formalisms.

C. Intrinsic point defects in bcc Cr

In Cr, point defect properties were determined for both nonmagnetic and antiferromagnetic bcc configurations. The formation energies are reported in Table IV. The magnetic state does not have a significant influence on the formation energies which are generally larger than in bcc Fe. The vacancy formation energy is more than 0.5 eV larger than that in Fe and in agreement with other DFT calculations.[32] Isomorphous phase separation occurs for Fe-Cr alloys with Cr concentrations larger than 10%. The Fe-rich α phase coexists with the Cr-rich α' phase at intermediate temperatures. As a result of the large difference in formation energies in such a phase separated alloy, vacancies will remain preferentially inside the Fe-rich matrix and will not diffuse easily into the Cr precipitates.

The most stable configuration for self-interstitials is the ⟨110⟩ configuration, as in Fe. The energy difference between the ⟨111⟩ and ⟨110⟩ interstitials is 15 meV for a 128 atom nonmagnetic supercell using PAW and 100 meV using

TABLE III. Local magnetic moment (in μ_B) on nearest-neighbor atoms for vacancy and Cr in substitutional position (for bcc Fe, $\mu_{PAW}=2.21\mu_B$ and $\mu_{USPP}=2.53\mu_B$).

Configuration	Position	PAW	USPP
Vacancy	1nn	2.45	2.70
	2nn	2.12	2.41
Cr subs	Cr	−1.64	−2.46
	1nn	2.20	2.43
	2nn	2.22	2.41

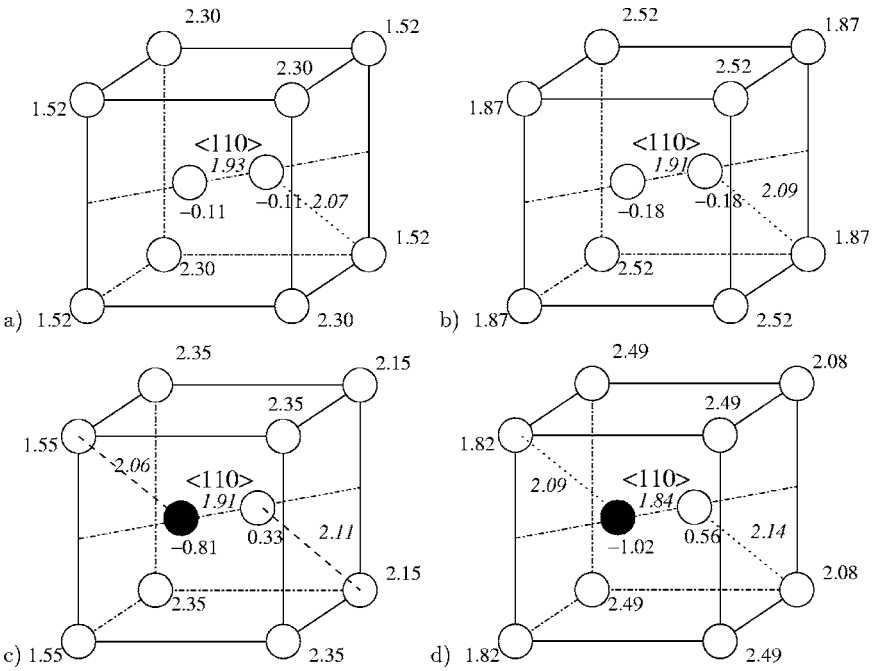

FIG. 1. Local magnetic moment (in μ_B) of $\langle 110 \rangle$ dumbbell and of $\langle 110 \rangle$-Cr mixed dumbbell ($\langle 110 \rangle_{\text{Fe-Cr}}$) using PAW (a,c) and USPP (b,d) 54 atom supercell. The relaxed distances in Å are indicated in italic.

USPP. For the AF structure, the difference is 44 meV for PAW. The small directional stability of the $\langle 110 \rangle$ interstitial with respect to that in iron can be explained by magnetic effects. The magnetic relaxation in pure iron allows for a lower formation energy of the $\langle 110 \rangle$ dumbbell than that in pure Cr. For nonmagnetic bcc transition metals, like vanadium and molybdenum, the order of directional stability is reversed.[33,34]

The formation energies of interstitials are more than 1 eV larger than those in Fe. The consequence for radiation damage of Fe-Cr alloys is that interstitial defects will diffuse preferentially in the Fe matrix and will not diffuse into existing large Cr precipitates (α' phase). Thus, in segregated alloys, the effective path to the grain boundary will be longer as the interstitials experience more scattering than in a single phase matrix. Moreover, interstitial clusters of $a/2\langle 111 \rangle$ type which do not turn easily from their glide plane may be trapped between precipitates.

D. Cr substitution and atomic relaxation

The energy of substitution is defined as the formation energy [of Eq. (2.2)] with one Cr atom in substitutional posi-

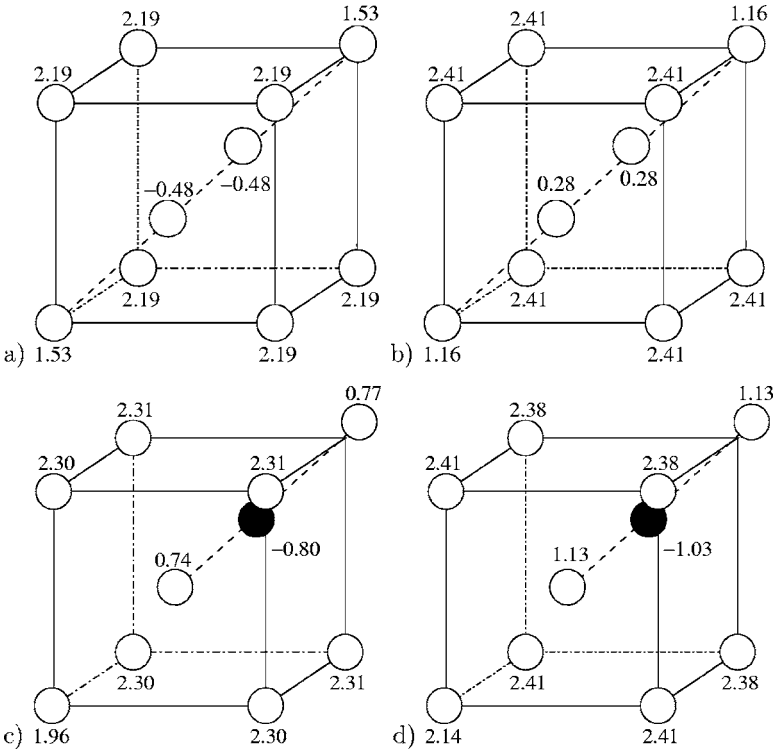

FIG. 2. Local magnetic moment (in μ_B) of $\langle 111 \rangle$ crowdion and of $\langle 111 \rangle$-Cr complex ($\langle 111 \rangle_{\text{Fe-Cr}}$) using PAW (a,c) and USPP (b,d) 54 atom supercell.

TABLE IV. Point defect formation energy (eV) in pure bcc Cr nonmagnetic (NM) and antiferromagnetic (AF), USPP and PAW calculations with 54 atom supercells and 125 k points and 128 atom supercells and 27 k points.

	PAW (NM)		PAW (AF)		USPP (NM)		USPP (AF)
Defect	54 at.	128 at.	54 at.	128 at.	54 at.	128 at.	54 at.
Vacancy	2.59	2.61	2.81	2.71	2.60	2.52	2.81
⟨100⟩	6.78	6.75	6.79	6.71	6.53	6.59	6.77
⟨110⟩	5.66	5.62	5.73	5.66	5.36	5.29	5.65
⟨111⟩	5.68	5.63	5.77	5.70	5.45	5.39	5.84
Octahedral	6.91	6.78	6.92	6.73	6.68	6.54	6.79
Tetrahedral	6.50	6.35	6.54	6.31	6.28	6.09	–

tion in bcc Fe. The substitution energy of Cr is −0.12 eV using PAW and −0.46 eV for USPP. The large difference of 0.3 eV between the two methods is due to the difference in the relaxation of the magnetic moment of the substitutional Cr atom. The PAW method gives an antiferromagnetic moment of $-1.59\mu_B$ while USPP gives $-2.40\mu_B$. Different measurements of the local Cr moment range between −0.7 and $-1.4\mu_B$,[35–37] in support of the prediction made by the PAW method. The relaxation of Fe atoms close to a substituted Cr atom is small, and only the first shell of Fe atoms have a very weak relaxation of 0.2–0.3 % of the first nearest-neighbor distance towards the Cr atom, using either formalism. This small relaxation is coherent with the small size factor of Cr in Fe (4.4% oversized[38]). The apparent discrepancy regarding the sign of the relaxation is not significant with so small a size difference, and the relaxation may change with temperature due to the relative difference in vibrational properties of Fe and Cr.

E. Mixing energies

Table V gives the mixing energy as a function of the Cr concentration. The mixing energy is obtained using Fe supercells of different size including one or a few Cr atoms. For 1.85%, it is one Cr atom with 53 Fe atoms. For 6.25%, it is one Cr atom with 15 Fe atoms. For 12.5%, it is two Cr atoms with 14 Fe atoms [Cr at (0,0,0) and (0.5 0.5 0.5) in reduced units]. For 25%, it is four Cr atoms with 12 Fe atoms [Cr at $(\frac{1}{4},\frac{1}{4},\frac{3}{4})$, $(\frac{1}{4},\frac{3}{4},\frac{1}{4})$, $(\frac{3}{4},\frac{1}{4},\frac{1}{4})$, and $(\frac{3}{4},\frac{3}{4},\frac{3}{4})$ in reduced units]. The results are also compared to *ab initio* calculations based on the coherent potential approximation (CPA).[39] The mixing energy is negative for very low Cr concentrations and become positive for larger Cr concentrations. The values obtained using USPP are similar to those from the CPA calculations while the values obtained using PAW are in average smaller. The comparison with the CPA results are mostly qualitative as the methods of calculation differ significantly. The CPA is a single-site mean field approximation which treats the solute concentration as a continuous variable while the PAW and USPP results are obtained using supercells of different sizes, thus enforcing slightly ordered structures at fixed concentrations. For a thorough study of mixing enthalpies of ordered structures in Fe-Cr, see the work by Klaver *et al.*[40]

TABLE V. Fe-Cr mixing energy (meV) (16 atom supercell with $7\times7\times7$ k points, 54 atom supercell with $5\times5\times5$ k points). Comparison is made with CPA calculations (Ref. 39).

Cr (%)	PAW	USPP	CPA[a]
1.85	−0.86	−6.56	−4.46
6.25	−1.95	−14.5	−7.59
12.5	6.10	11.1	−7.21
25.0	59.6	71.2	45.3

[a]Reference 39.

F. Cr defect interaction in bcc Fe

1. Cr substitutional interactions

Interactions between Cr atoms and vacancies as well as between Cr atoms in substitutional positions have been calculated. Binding and formation energies are presented in Table VI using 54 and 128 atom supercells.

The vacancy-Cr (VCr) binding energy is small, about 60 meV in the first-nearest-neighbor position and vanishing for larger separation distances. These results are in agreement with the experimental results of Möslang *et al.*[41] Using muon spectroscopy, they have estimated the VCr binding energy to be less than 105 meV. Furthermore, isochronal annealing measurements showed that the vacancy migration occurs almost at the same temperature (200 K) in pure Fe as in the Fe-Cr alloy.[42] The difference with respect to predictions using USPP is small when it comes to Cr-vacancy interactions.[43]

Cr atoms in bcc Fe have a lower barrier for vacancy assisted migration than Fe atoms do (Table VII). The migration energy is 0.17 eV lower for solute Cr than for the matrix atoms.

Figure 3 displays the Cr cluster configurations that were investigated. Cr-Cr interactions are repulsive for all small Cr clusters considered (up to size four). Thus the binding energies are negative and are increasing with the number of Cr -Cr pairs formed. Both USPP and PAW lead to negative binding energies, the repulsion is nevertheless smaller with PAW than with USPP. This difference is consistent with the difference in the substitutional energy. In PAW, a substitu-

TABLE VI. Binding and formation energies (eV) of VCr pairs, Cr clusters, ⟨100⟩-Cr, ⟨110⟩-Cr, and ⟨111⟩-Cr complexes using the PAW method (54 atom supercell, 125 k points, 128 atom supercell, 27 k points). The reference energies are pure bcc Fe and pure nonmagnetic bcc Cr, respectively.

	Binding energy		Formation energy	
Configuration	54 at.	128 at.	54 at.	128 at.
V-Cr 1nn	0.057	0.057	1.95	1.98
V-Cr 2nn	0.007	0.014	2.00	2.02
Cr+Cr 1nn	−0.233	−0.242	0.01	0.02
Cr+Cr 2nn	−0.148	−0.123	−0.08	−0.10
Cr+Cr+Cr (triangle)	−0.496	−0.477	0.15	0.15
Cr+Cr+Cr+Cr (tetrahedral)	−0.728	−0.710	0.26	0.27
$\langle 100\rangle_{\text{Fe-Cr}}$	0.153	0.097	5.10	4.93
$\langle 110\rangle_{\text{Fe-Cr}}$	0.059	0.080	3.96	3.83
$\langle 111\rangle_{\text{Fe-Cr}}$	0.385	0.373	4.39	4.24
Octa-Cr	0.297	0.298	5.10	4.88
Tetra-Cr	0.020	0.074	4.43	4.26
$\langle 110\rangle_{\text{Fe-Fe}} \perp \text{Cr}_{subs}$	−0.080	−0.065	4.10	3.98
$\langle 110\rangle_{\text{Fe-Fe}} - \text{Cr}_{subs}$	0.051	0.050	3.97	3.86
$\langle 100\rangle_{\text{Cr-Cr}}$	−0.294	−0.356	5.43	5.27
$\langle 110\rangle_{\text{Cr-Cr}}$	−0.442	−0.425	4.35	4.23
$\langle 111\rangle_{\text{Cr-Cr}}$	0.247	0.223	4.42	4.28
$\langle 110\rangle_{\text{Fe-Cr}} \perp \text{Cr}_{subs}$	−0.057	−0.023	3.96	3.82
$\langle 110\rangle_{\text{Fe-Cr}} - \text{Cr}_{subs}$	−0.230	−0.209	4.14	4.01
$\langle 110\rangle_{\text{Cr-Fe}} - \text{Cr}_{subs}$	0.131	0.154	3.78	3.65
$\text{Cr}_{subs} - \langle 110\rangle_{\text{Fe-Fe}} \perp \text{Cr}_{subs}$	−0.072	−0.041	3.98	3.84
$\langle 110\rangle_{\text{Fe-Fe}} - \text{Cr}^{2nn}_{subs}\text{Cr}_{subs}$	0.061	0.094	3.84	3.71
$\langle 110\rangle_{\text{Fe-Fe}} - \text{Cr}^{3nn}_{subs}\text{Cr}_{subs}$	0.146	0.154	3.76	3.65
$\langle 110\rangle_{\text{Fe-Fe}} - \text{Cr}^{5nn}_{subs}\text{Cr}_{subs}$	0.112	0.118	3.79	3.68
$\langle 110\rangle_{\text{Fe-Fe}} \perp \text{Cr}^{2nn}_{subs}\text{Cr}_{subs}$	−0.258	−0.195	4.16	4.00
$\langle 110\rangle_{\text{Fe-Fe}} \perp \text{Cr}^{3nn}_{subs}\text{Cr}_{subs}$	−0.157	−0.121	4.06	3.92
$\langle 110\rangle_{\text{Fe-Fe}} \perp \text{Cr}^{5nn}_{subs}\text{Cr}_{subs}$	−0.172	−0.123	4.08	3.92
$\langle 111\rangle_{\text{Cr-Fe-Cr}}$	0.549	0.544	4.12	3.95

tional Cr atom does not cause as large a perturbation as in USPP. The decrease of the total binding energy is smaller than the value given by adding all the first-nearest-neighbor (1nn) and second-nearest-neighbor (2nn) interactions $[2E_b(\text{Cr-Cr 1nn})+E_b(\text{Cr-Cr 2nn})$ for the Cr_3 cluster and $4E_b(\text{Cr-Cr 1nn})$ for the Cr_4 cluster]. This screening behavior, which was not observed for Cu in Fe,[44] is probably due to magnetic effects, as Cr carries a local magnetic moment whereas Cu does not.

TABLE VII. Fe and Cr migration energies in eV (54 atom supercell with 125 k points, 128 atom supercell with 27 k points).

	54 atoms	128 atoms
E_{mig}(Fe)	0.69	0.71
E_{mig}(Cr)	0.54	0.54

2. Cr–self-interstitial interactions

The interactions of one and two Cr atoms with ⟨100⟩, ⟨110⟩, and ⟨111⟩ self-interstitials have been studied considering different possible configurations described in Fig. 4. The binding and formation energies are presented in Table VI.

For the mixed interstitials, the $\langle 100\rangle_{\text{Fe-Cr}}$ and $\langle 110\rangle_{\text{Fe-Cr}}$ configurations have small binding energies while the $\langle 111\rangle_{\text{Fe-Cr}}$ crowdion is more strongly bound. The binding energy for the $\langle 110\rangle_{\text{Fe-Cr}}$ configuration is close to zero using USPP, whereas is it around 0.1 eV using PAW. For the $\langle 111\rangle_{\text{Fe-Cr}}$ configuration the calculated binding energy is about 0.4 eV with both methods.[43]

The 0.4 eV binding energy between the ⟨111⟩ crowdion and the Cr atom, reduces the $\langle 111\rangle_{\text{Fe-Cr}}$ formation energy, thus reducing the ⟨111⟩−⟨110⟩ energy difference by 0.36 eV. In pure Fe the large energy difference of 0.7 eV between ⟨111⟩ and ⟨110⟩ configurations, induce a preferential migration of the ⟨110⟩ interstitial through the migration and rotation mechanism[8] previously suggested by Johnson.[45] The consequence of the presence of Cr may be both trapping and an increase of directional change probability during the gliding of the ⟨111⟩ crowdion.

For the ⟨100⟩ interstitials, it is only the $\langle 100\rangle_{\text{Fe-Cr}}$ configuration which is binding. Placing further Cr atoms in proximity to the ⟨100⟩ interstitial is either unfavorable or simply renders the same effect as the mixed $\langle 100\rangle_{\text{Fe-Cr}}$ configuration. A configuration with a Cr atom in first-nearest-neighbor position to an $\langle 100\rangle_{\text{Fe-Fe}}$ or $\langle 100\rangle_{\text{Fe-Cr}}$ interstitial is unstable enough that the interstitial turns to the more stable ⟨110⟩ direction during a self-consistent ionic relaxation. The octahedral and tetrahedral mixed interstitials are also bound but there is no evidence in the literature of them playing a significant role in the evolution of the microstructure. In the

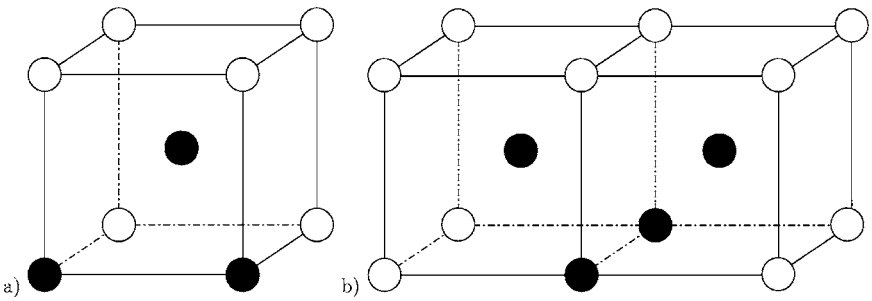

FIG. 3. Cr clusters with (a) Cr_3: three Cr atoms and (b) Cr_4: four Cr atoms. The Cr position is indicated by the black circle.

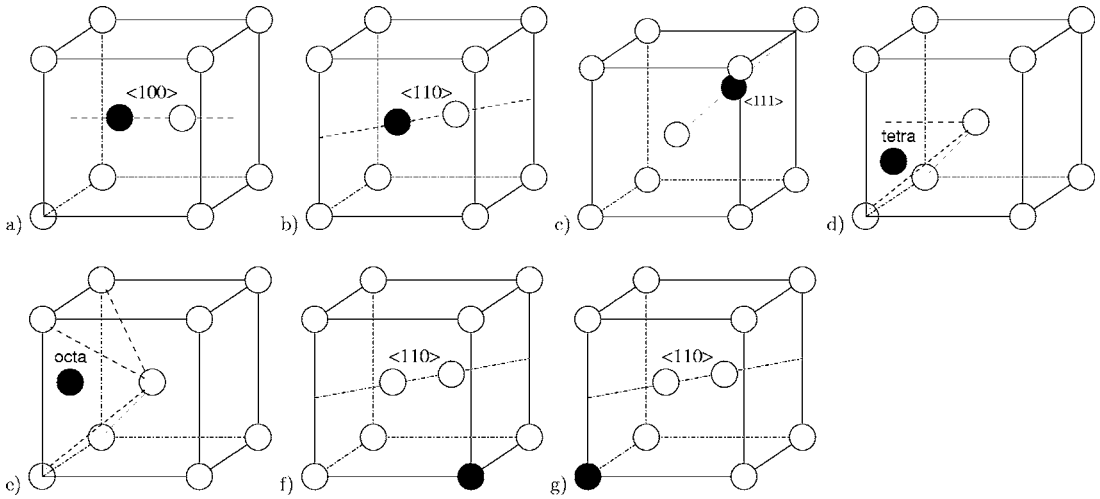

FIG. 4. SIA-Cr configurations: (a) Fe-Cr ⟨100⟩ dumbbell ($\langle 100\rangle_{\text{Fe-Cr}}$). (b) Fe-Cr ⟨110⟩ dumbbell ($\langle 110\rangle_{\text{Fe-Cr}}$). (c) Fe-Cr ⟨111⟩ dumbbell ($\langle 111\rangle_{\text{Cr-Cr}}$). (d) Fe-Cr tetrahedral interstitial. (e) Fe-Cr octahedral interstitial. (f) Cr near ⟨110⟩ dumbbell at the site under tension ($\langle 110\rangle_{\text{Fe-Fe}} \perp \text{Cr}_{subs}$). (g) Cr near ⟨110⟩ dumbbell at the site under compression ($\langle 110\rangle_{\text{Fe-Fe}} - \text{Cr}_{subs}$). The Cr position is indicated by the black circle.

case of the octahedral symmetry, the formation energy is too large for it to exist long enough to matter. For the tetrahedral defect, the small binding energy and unfavorable symmetry, in terms of forming defect clusters, diminishes the importance of this type of defect. On the macroscopic scale, the effects of ⟨100⟩, octahedral, and tetrahedral interstitials interacting with Cr atoms will be small.

The interaction of Cr with ⟨110⟩ in the tensile site ($\langle 110\rangle_{\text{Fe-Fe}} \perp \text{Cr}_{subs}$) is slightly repulsive. A Cr atom with ⟨110⟩ in the nearest-neighbor compression site ($\langle 110\rangle_{\text{Fe-Fe}} - \text{Cr}_{subs}$) has a slightly positive binding energy.

For the mixed ⟨110⟩ dumbbell ($\langle 110\rangle_{\text{Fe-Cr}}$) the relaxed Fe-Cr distance is smaller than the Fe-Fe distance in the pure Fe ⟨110⟩ dumbbell (Fig. 1). This effect, which cannot be explained by the fact that a Cr atom within the Fe matrix is slightly oversized,[38] may be consistent with the magnetic interactions discussed below.

In the case of a single Cr atom interacting with a defect, the binding energies obtained with PAW are on average 0.1 eV larger than those from USPP. Since the substitutional energy of Cr enters the expression for the binding energy in an additive manner, the difference in binding with respect to only the defect structure is actually 0.2 eV smaller with PAW than with USPP. Since the PAW substitution energy is small, the binding energies obtained with PAW are mainly due to the effects of structural perturbations and magnetic relaxation.[43]

The origin of the affinity of Cr with self-interstitial atoms is not obvious. Since the formation energy of self-interstitials in bcc Cr has been found to be 1 eV larger than for self interstitials in bcc Fe, a repulsion would be expected rather than the attraction obtained. However, as only one Cr atom is involved in the bcc matrix, the chemical interaction between Fe and Cr atoms is more predominant than the highly strained behavior seen in pure Cr.

The obtained binding interaction between self-interstitial atoms and Cr is consistent with electrical resistivity measurement of low-temperature electron irradiated Fe-Cr alloys.[46] Maury *et al.*[46] interpreted the faster recovery behavior at stage I as the formation of mixed dumbbells with a higher mobility than self-interstitial atoms in Fe have. This may also be due to the low directional stability of the mixed dumbbell in comparison to that of a pure Fe SIA.

Figure 5 shows the configurational stability of interstitial defects with or without Cr atoms as central parts of the defect. For pure Fe, the curve is basically identical to recently published results[34] where the anomalous behavior of Fe was discussed in comparison with the other bcc metals. Only in ferromagnetic Fe is the ⟨111⟩ not the most stable defect. The magnetic interactions in Fe raises the energy of the ⟨111⟩ interstitial with respect to the other configurations. As can be seen in Fig. 5, the inclusion of Cr in the defect diminishes

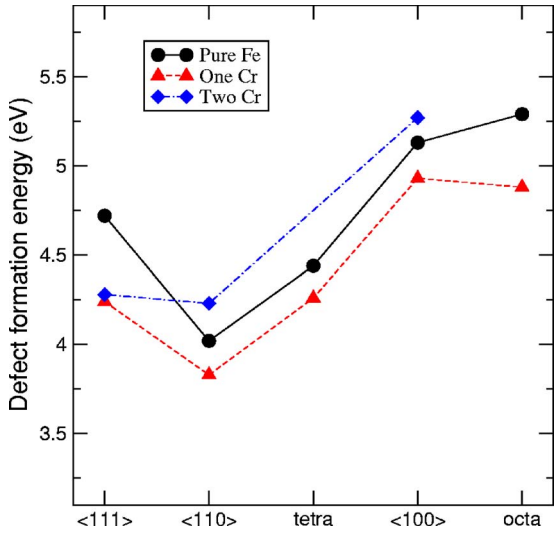

FIG. 5. (Color online) The formation energies of the different interstitials in Fe. The circles represent pure Fe, the triangles when one Cr atom is in the defect, and the diamonds when two Cr atoms are in the defect.

the difference between the ⟨111⟩ and the other configurations. The reason being that Cr is much more magnetically malleable than Fe. Note especially how the difference between the two main directions is almost vanishing when two Cr atoms occupy the defect sites. This may affect the interstitial diffusion pathways substantially as the directional stability, which is a main feature in pure Fe, can be cancelled out in a concentrated alloy. The order of stability for the two-Cr defect configurations in Fe is almost identical to that of self-interstitials in pure Cr. Furthermore, it can be seen that the only other point which diverges slightly is the octahedral mixed interstitial. This configuration is slightly more favorable than the pure ⟨100⟩ interstitial for symmetry reasons that are not present in the case of a pure defect.

Figure 6 represents the Cr positions of the two Cr atoms investigated relative to the ⟨100⟩, ⟨110⟩, and ⟨111⟩ dumbbells.

The binding energies are generally found to be lower when two Cr atoms are associated with an Fe self-interstitial as compared to when one single Cr atom is interacting with the Fe self-interstitial. This is coherent with the repulsion between two Cr atoms in substitutional positions. Only for configurations with a large distance between the Cr atoms is it possible to use simple summation of the binding energies of the respective one-Cr defect configurations. For configurations where the distance between the Cr atoms is small enough, the repulsion plays a more and more important role. For a configuration XY with two Cr atoms the binding energy can be written as

$$E_b(XY) = E_b(X) + E_b(Y) - E_{rep}(d), \tag{3.1}$$

where $E_b(X)$ is the binding energy of configuration X containing the defect and one Cr atom and $E_{rep}(d)$ is the pair repulsion energy for two Cr atoms displaced by the distance d. Configurations with more than two Cr atoms in close proximity to the defect have not been considered in this study but the same reasoning could probably be expanded to cases with any number of Cr atoms, as long as one stays within the α phase of the alloy. Figure 7 shows the Cr pair repulsion, defined by Eq. (3.1). The black circles are calculated data points, the solid line is a fit to a smooth exponential function with two terms. The vertical dashed lines displays the unperturbed nearest-neighbor positions. This simple model captures both the positive and negative parts of the Cr pair repulsion. Although it has no physical meaning, one can still argue that since it does not capture the Cr pair repulsion present in defect free systems, something else is happening there. The apparent discrepancy between the Cr pair repulsion in defect-free configurations and in configurations with an interstitial can be explained by magnetic effects. In the interstitial systems the magnetic interactions are somewhat reduced by the defect induced strain whereas in defect-free configurations the magnetic interactions are prominently responsible for the strong Cr repulsion.[40]

For two Cr atoms and a ⟨110⟩ dumbbell, the most stable configuration is $\langle 110\rangle_{\text{Cr-Fe}} - \text{Cr}_{subs}$ where the two most stable single-Cr configuration, namely $\langle 110\rangle_{\text{Fe-Cr}}$ and $\langle 110\rangle_{\text{Fe-Fe}} - \text{Cr}_{subs}$, have been combined while keeping the distance between the Cr atoms as large as possible. This configuration has a 0.2 eV binding energy using PAW and vanishing using USPP. The most repulsive configuration is the Cr dumbbell $\langle 110\rangle_{\text{Cr-Cr}}$ both using PAW and USPP (−0.3 and −0.4 eV) for which the Cr atoms are the closest. The configuration $\langle 110\rangle_{\text{Fe-Cr}} - \text{Cr}_{subs}$ is also unfavorable since the Cr atoms are at a sufficiently small distance to allow the Cr-pair repulsion to dominate over the attraction present for the single-Cr configurations to which it can be reduced. Furthermore, the configuration $\langle 110\rangle_{\text{Fe-Cr}} \perp \text{Cr}_{subs}$ is slightly repulsive using USPP and with zero binding energy using PAW.[43]

The complex formed by two Cr atoms in a ⟨111⟩ crowdion with an Fe atom between the two Cr atoms ($\langle 111\rangle_{\text{Cr-Fe-Cr}}$) has a stronger binding energy (0.6 and 0.4 eV with PAW and USPP, respectively) than when the Cr atoms are nearest neighbors ($\langle 111\rangle_{\text{Cr-Cr}}$) (0.3 and 0.1 eV with PAW and USPP, respectively), also in line with the Cr pair repulsion model.

The binding energies of configurations containing two Cr atoms and a defect are on average 0.26 eV larger with PAW than with USPP. The main reason for the repulsive interactions predicted by USPP is the large negative substitution energy. The large difference in the binding energy of the $\langle 111\rangle_{\text{Cr-Cr}}$ using PAW (0.3 eV) and USPP (0.06 eV) again suggests that PAW is more consistent with experiments that indicate the formation of Cr-Cr interstitials in concentrated Fe-Cr alloys.[47]

The high binding energies of the ⟨111⟩ complexes will lead to a trapping of interstitial $a/2\langle 111\rangle$ loops by Cr atoms.[48] This extrapolation of the *ab initio* results may be coherent with the observation of the existence of $a/2\langle 111\rangle$ loops by transmission electron microscope experiments for high Cr concentrations.[5] The probability to have Cr atoms around third nearest-neighbor distance is significant for Cr concentrations larger than 10%. Thus the trapping, or at least the reduction of the mobility, of interstitial clusters may be efficient enough to nucleate the observed $a/2\langle 111\rangle$ loops.

The ensuing reduction of mobility of the ⟨111⟩ loops, as discussed by Terentyev *et al.*, is probably the main contributor to the decrease in the neutron induced swelling of Fe-Cr alloys as compared to that in pure iron.[48]

3. Magnetism

Since the magnetic moment is strongly perturbed for point defects in pure bcc Fe,[7,49] as shown for both the PAW and USPP methods described above, the local magnetic moment has been analyzed for Cr atoms.

The local magnetic moment on Cr atoms for different configurations is given in Table VIII and indicated in Figs. 1, 2, 6, and 8. For most of the configurations with Cr in substitutional position, the Cr atom has an antiferromagnetic moment, as compared to that in the Fe matrix, of around $-2.4\mu_B$ using USPP and $-1.6\mu_B$ using PAW. When Cr is in interstitial position the magnetic moment is strongly reduced, and even more so for two Cr atoms in the interstitial dumbbell.

The presence of substitutional Cr only slightly perturbs the local moment on the nearest-neighbor Fe atoms. For example, in Table III, it can be seen that the moment on the

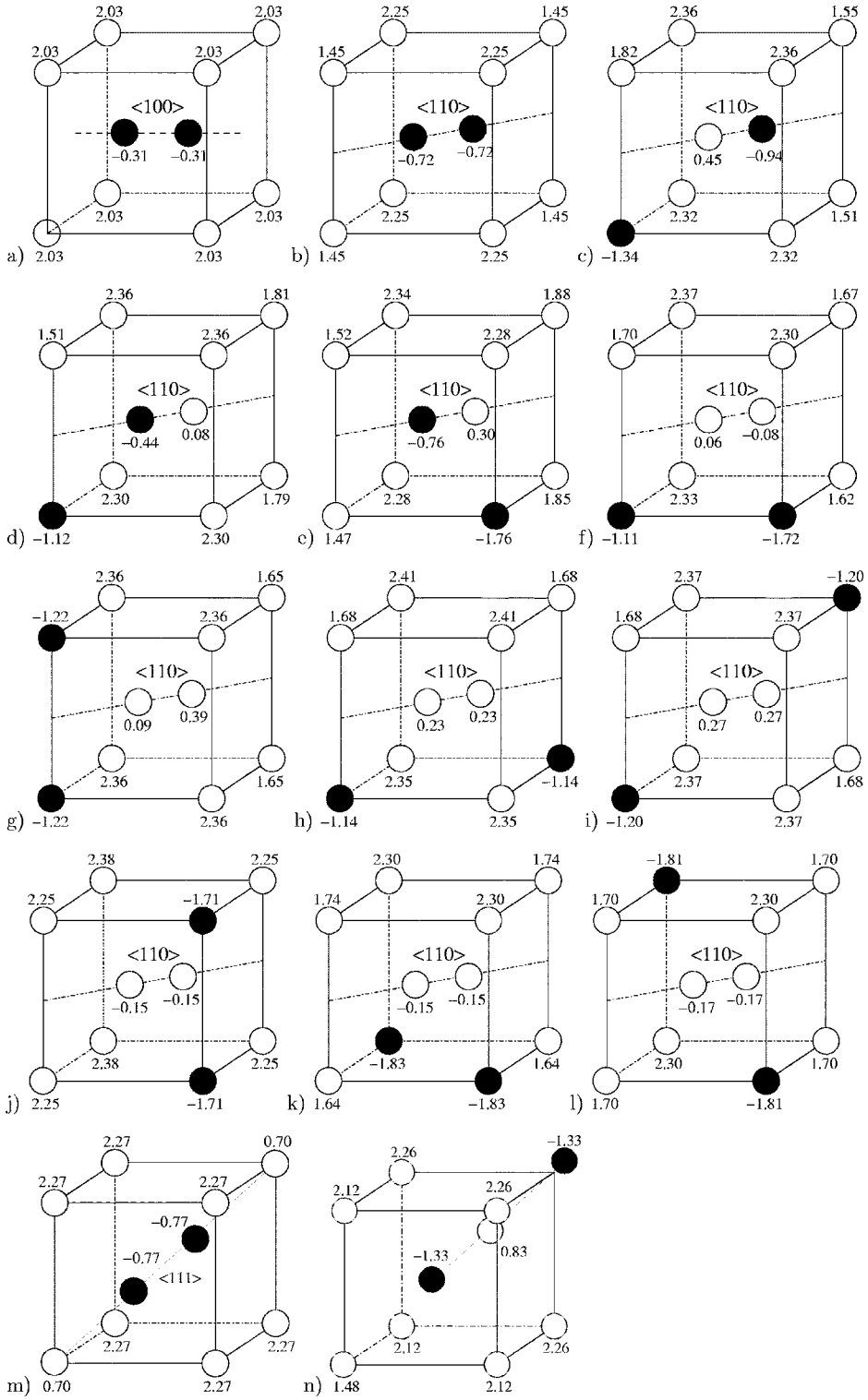

FIG. 6. SIA—two Cr configurations. (a) Cr substituted ⟨100⟩ dumbbell ($\langle 100\rangle_{\text{Cr-Cr}}$). (b) Cr substituted ⟨110⟩ dumbbell ($\langle 110\rangle_{\text{Cr-Cr}}$). (c) Mixed ⟨110⟩ dumbbell and Cr in the far compression site ($\langle 110\rangle_{\text{Cr-Fe}} - \text{Cr}_{subs}$). (d) Mixed ⟨110⟩ dumbbell and Cr in the near compression site ($\langle 110\rangle_{\text{Fe-Cr}} - \text{Cr}_{subs}$). (e) Mixed ⟨110⟩ dumbbell and Cr in tension site ($\langle 110\rangle_{\text{Fe-Cr}} \perp \text{Cr}_{subs}$). (f) One Cr in compression site and one in tension site around ⟨110⟩ dumbbell ($\text{Cr}_{subs} - \langle 110\rangle_{\text{Fe-Fe}} \perp \text{Cr}_{subs}$). (g) Two Cr in 2nn compression sites in front of a ⟨110⟩ dumbbell ($\langle 110\rangle_{\text{Fe-Fe}} - \text{Cr}^{2nn}_{subs}\text{Cr}_{subs}$). (h) Two Cr in 3nn compression sites around with ⟨110⟩ dumbbell ($\langle 110\rangle_{\text{Fe-Fe}} - \text{Cr}^{3nn}_{subs}\text{Cr}_{subs}$). (i) Two Cr in 5nn compression sites around ⟨110⟩ dumbbell ($\langle 110\rangle_{\text{Fe-Fe}} - \text{Cr}^{5nn}_{subs}\text{Cr}_{subs}$). (j) Two Cr in 2nn tension sites around ⟨110⟩ dumbbell ($\langle 110\rangle_{\text{Fe-Fe}} \perp \text{Cr}^{2nn}_{subs}\text{Cr}_{subs}$). (k) Two Cr in 3nn tension sites around ⟨110⟩ dumbbell ($\langle 110\rangle_{\text{Fe-Fe}} \perp \text{Cr}^{3nn}_{subs}\text{Cr}_{subs}$). (l) Two Cr in 5nn tension sites around ⟨110⟩ dumbbell ($\langle 110\rangle_{\text{Fe-Fe}} \perp \text{Cr}^{5nn}_{subs}\text{Cr}_{subs}$). (m) Cr substituted ⟨111⟩ dumbbell ($\langle 111\rangle_{\text{Cr-Cr}}$). (n) Cr substituted ⟨111⟩ crowdion ($\langle 111\rangle_{\text{Cr-Fe-Cr}}$). The local magnetic moment (in μ_B) for the PAW calculation is indicated. The Cr position is indicated by the black circle.

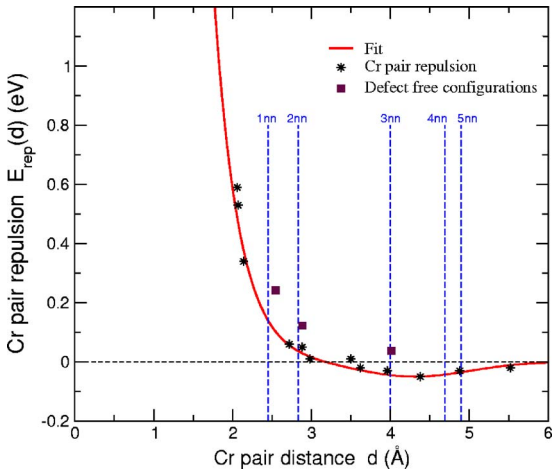

FIG. 7. (Color online) The Cr pair repulsion, as defined by Eq. (3.1) is shown by stars for the configurations which include an interstitial. A fit to this data is shown as a solid line. The Cr pair repulsion for configurations without defects are shown as filled boxes. The unperturbed nearest-neighbor distances in Fe are displayed by the dashed vertical lines.

first- and second-nearest-neighbor Fe atoms is not affected significantly in either PAW or USPP calculations.

For most interstitial-Cr complexes, the local magnetic moments are significantly quenched on the Fe atoms that are closest to the Cr atoms. The exceptions are for the most stable configurations $\langle 110\rangle_{\text{Fe-Cr}}$, $\langle 111\rangle_{\text{Fe-Cr}}$, and $\langle 111\rangle_{\text{Cr-Fe-Cr}}$, which are displayed in Figs. 1, 2, and 8. For these configurations, the local magnetic moment of the Fe atom in interstitial position is no longer antiferromagnetic or close to zero. Rather, a positive local magnetic moment is carried (around $0.5\mu_B$ using PAW and $1\mu_B$ using USPP).

For the less stable configurations, with negative or very small binding energies, the local magnetic moment on the Cr atoms is very small. Moreover, in these cases, the local magnetic moment on Fe atoms is slightly quenched by the presence of the nearby Cr atoms and the defect.

Despite the reduction of the antiferromagnetic character of Cr in interstitial configurations, it can lead to a favorable situation as compared to Fe self-interstitials and substitutional Cr. The penalty is compensated by the increase of the nearby Fe magnetic moments by anti-ferromagnetic coupling, which induce a smaller perturbation than the small negative Fe moment in self-interstitials. With two Cr in second nearest position (with an Fe atom in between), the antiferromagnetic character of Cr atoms is reinforced and the configurations are stabilized ($\langle 110\rangle_{\text{Cr-Fe}}-\text{Cr}_{subs}$ or $\langle 111\rangle_{\text{Cr-Fe-Cr}}$).

Furthermore, the antiferromagnetic character of the interaction between Cr atom within the $\langle 110\rangle$ dumbbell and the nearest Fe atoms can explain the shorter interatomic distance as compared to in the $\langle 110\rangle$ self-interstitial.

IV. CONCLUSIONS

A study of the energetic and magnetic character of intrinsic point defects in bcc Fe and bcc Cr has been performed. Furthermore, the interaction of Cr atoms with point defects in bcc iron has been characterized. Two *ab initio* formalisms, the projector augmented wave (PAW) method and the ultrasoft pseudopotential (USPP) approach, have been used throughout this study.

The following conclusions can be made:

(1) The negative energy of substitution for Cr in bcc Fe, which differs by 0.3 eV between PAW and USPP, is a very important factor in the determination of binding energies for point defect complexes with Cr atoms. Fewer defect configurations have binding character using USPP than PAW, since USPP predicts a larger negative value of the substitution energy. The difference between the values obtained with PAW and with USPP can be related to the difference in the magnetic moment on the solute Cr atom.

(2) The magnetic interactions are strongly coupled with the binding or repulsive character of the defect configuration. If the magnetic moments are significantly quenched then the configuration is more repulsive than if they stay closer to the bulk values. Configurations containing Cr atoms are binding if the Cr atoms have large antiferromagnetic moments, in accordance with the moment of a single Cr atom in bcc Fe. Furthermore, the binding energies of configurations with two Cr atoms and an interstitial can be described as additive with respect to the binding energies of single-Cr defect configurations with a smooth correction term depending on the Cr pair distance. That this does not work for defect-free configurations indicates that the magnetic interactions are stronger there.

(3) During the relaxation phase of displacement cascades in Fe-Cr, the created interstitial defects will gradually be attracted to solute Cr atoms and form mixed Fe-Cr and substitutional Cr-Cr interstitials, in agreement with experimental evidence.

(4) Of the two formalisms, the full-potential PAW method should be chosen over the USPP since the PAW is more physically correct and results obtained with it correlate better with experiments. This is especially true for transition metals and alloys where delicate magnetic interactions play an important role. The main difference between the results obtained with the two formalisms is connected to the local magnetic moments. In the case of pure iron, the methods

TABLE VIII. Local magnetic moment (in μ_B) on Cr atoms in different configurations.

Configuration	128 at. PAW	128 at. USPP
Cr subs	−1.71	−2.28
Cr migration	−1.99	−2.58
V-Cr 1nn	−1.99	−2.52
V-Cr 2nn	−1.85	−2.36
Cr+Cr 1nn	−1.39	−2.12
Cr+Cr 2nn	−1.58	−2.16
$\langle 110\rangle_{\text{Fe-Cr}}$	−0.81	−1.06
$\langle 111\rangle_{\text{Fe-Cr}}$	−0.80	−1.16
$\langle 110\rangle_{\text{Cr-Cr}}$	−0.72	−0.27
$\langle 111\rangle_{\text{Cr-Cr}}$	−0.77	−0.38

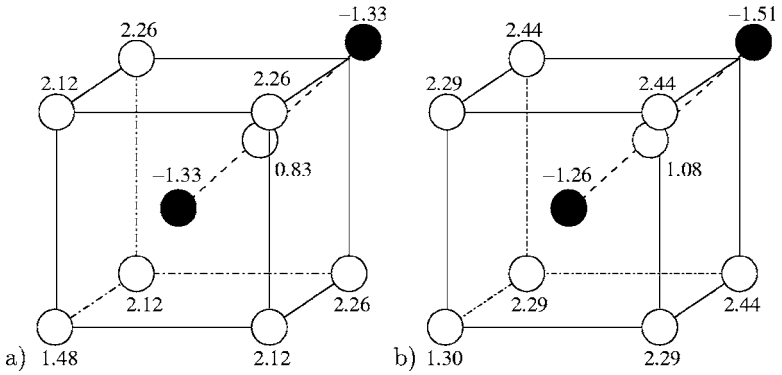

FIG. 8. Local magnetic moment (in μ_B) for $\langle 111\rangle$-2Cr dumbbell configuration ($\langle 111\rangle_{\text{Cr-Fe-Cr}}$) using (a) PAW and (b) USPP, 54 atom supercell.

give similar results although the USPP method overestimates the bulk moment. The largest difference in pure Fe is that PAW predicts an antiferromagnetic moment on the $\langle 111\rangle$ self-interstitial atoms while USPP does not. For pure chromium the difference is not large, as magnetism does not come into play to the same degree. However, for Cr atoms in bcc Fe, the difference is significant. For configurations with a single Cr atom, PAW predicts 0.1 eV larger binding energies than USPP does. Hence, some configurations which are bound with PAW are repulsive or essentially noninteracting with USPP. For configurations with two Cr atoms, PAW predicts binding energies which are about 0.3 eV larger than USPP. As a result, most two-Cr configurations are repulsive with USPP even if they are significantly bound with PAW.

Both methods predict very weak VCr interactions in agreement with experiment. The experimental data on interstitial migration suggests that mixed interstitials should migrate faster than pure Fe interstitials for alloys with low Cr content. The different character that PAW and USPP predicts in the interaction of Cr atoms with interstitial defects can not be conclusively linked to a pattern of interstitial migration without further study. Even though both methods predict the mixed $\langle 110\rangle_{\text{Fe-Cr}}$ dumbbell as the most stable defect with one Cr atom, the binding energy predicted by USPP is very small while PAW gives a reasonably significant binding. The experimental evidence of the existence of mixed dumbbells thus provides a further indication that the PAW method is the better description. Furthermore, the significant binding energy of the substitutional $\langle 111\rangle_{\text{Cr-Cr}}$ that PAW predicts is in agreement with experiments suggesting the formation of Cr-Cr interstitials in alloys with high Cr content.

(5) Cr-rich precipitates (α' phase) in Fe-Cr alloys will repel interstitial loops and will act as temporary sources of interstitials and vacancies. The larger interstitial formation energy in pure Cr, as compared to that in Fe, implies that interstitial diffusion will occur preferentially within the α phase of a phase separated alloy.

(6) The large binding interaction found for interstitial complexes, in either $\langle 110\rangle$ or $\langle 111\rangle$ direction, where two Cr atoms are separated by an Fe atom, may be correlated to the different type of interstitial loops observed experimentally as a function of the Cr content. The binding interaction between $\langle 111\rangle$ interstitials and Cr atoms will also slow down the diffusion of glissile interstitial loops. This should lead to an increased recombination with vacancies.

ACKNOWLEDGMENTS

The authors acknowledge fruitful discussions with Lorenzo Malerba, Sergei Simak, Peter Klaver, and Igor Abrikosov. This work has been partially supported by the European Commission within the project PERFECT (Contract No. FI6O-CT-2003-508840) and the ITEM network (Contract No. FIR1-CT-2001-20163). Part of the calculations were done on the supercomputers at Centre de Calcul Recherche et Technologie (CCRT) in the framework of an EDF-CEA contract. P.O. thanks the Swedish Research Council (VR) for financial support and the Swedish National Allocations Committee and the High Performance Computing Centre North for use of supercomputer facilities.

[1] E. A. Little and D. A Stow, J. Nucl. Mater. **87**, 25 (1979).
[2] D. S. Gelles, J. Nucl. Mater. **108&109**, 515 (1982).
[3] F. Garner, M. B. Toloczko, and B. H. Sencer, J. Nucl. Mater. **276**, 123 (2000).
[4] A. Koyama, A. Hishinuma, D. S. Gelles, R. L. Klueh, W. Dietz, and K. Ehrlich, J. Nucl. Mater. **233-237**, 138 (1996).
[5] S. I. Porollo, A. M. Dvoriashin, A. N. Vorobyev, and Yu. V. Konobeev, J. Nucl. Mater. **256**, 247 (1998).
[6] T. Konishi, K. Ohsawa, H. Abe, and E. Kuramoto, Comput. Mater. Sci. **14**, 108 (1999).
[7] C. Domain and C. S. Becquart, Phys. Rev. B **65**, 024103 (2001).
[8] C. C. Fu, F. Willaime, and P. Ordejón, Phys. Rev. Lett. **92**, 175503 (2004).
[9] L. Malerba, D. Terentyev, P. Olsson, R. Chakarova, and J. Wallenius, J. Nucl. Mater. **329**, 1156 (2004).
[10] D. Terentyev and L. Malerba, J. Nucl. Mater. **329**, 1161 (2004).
[11] J. Wallenius, P. Olsson, C. Lagerstedt, N. Sandberg, R. Chakarova, and V. Pontikis, Phys. Rev. B **69**, 094103 (2004).
[12] M. I. Mendelev, S. W. Han, D. J. Srolovitz, G. J. Ackland, D. Y. Sun, and M. Asta, Philos. Mag. **83**, 3977 (2003).
[13] G. J. Ackland, M. I. Mendelev, D. J. Srolovitz, S. Han, and A. V. Barashev, J. Phys.: Condens. Matter **16**, 1 (2004).

[14] P. Olsson, J. Wallenius, C. Domain, K. Nordlund, and L. Malerba, Phys. Rev. B **72**, 214119 (2005).
[15] P. Olsson, I. A. Abrikosov, L. Vitos, and J. Wallenius, J. Nucl. Mater. **321**, 84 (2003).
[16] G. Kresse and D. Joubert, Phys. Rev. B **59**, 1758 (1999).
[17] P. E. Blöchl, Phys. Rev. B **50**, 17953 (1994).
[18] D. Vanderbilt, Phys. Rev. B **41**, 7892 (1990).
[19] G. Kresse and J. Hafner, J. Phys.: Condens. Matter **6**, 8245 (1996).
[20] G. Kresse and J. Hafner, Phys. Rev. B **47**, 558 (1993).
[21] G. Kresse and J. Furthmüller, Phys. Rev. B **54**, 11169 (1996).
[22] G. Kresse and J. Furthmüller, Comput. Mater. Sci. **6**, 15 (1996).
[23] G. Kresse and D. Joubert, Phys. Rev. B **59**, 1758 (1999).
[24] J. P. Perdew, J. A. Chevary, S. H. Vosko, K. A. Jackson, M. R. Pederson, D. J. Singh, and C. Fiolhais, Phys. Rev. B **46**, 6671 (1992).
[25] S. H. Vosko, L. Wilk, and M. Nusair, Can. J. Phys. **58**, 1200 (1980).
[26] H. J. Monkhorst and J. D. Pack, Phys. Rev. B **13**, 5188 (1976). In the original Monkhorst and Pack scheme, the k point mesh is always symmetric around the Γ point, whereas very often in our calculations we adopted grids centred at the Γ point.
[27] E. Fawcett, H. L. Alberts, V. Yu. Galkin, D. R. Noakes, and J. V. Yakhmi, Rev. Mod. Phys. **66**, 25 (1994).
[28] R. Hafner, D. Spisak, R. Lorenz, and J.Hafner, J. Phys.: Condens. Matter **202**, 44 (2002).
[29] S. Cottenier, B. De Vries, J. Meersschaut, and M. Rots, J. Phys.: Condens. Matter **14**, 3275 (2002).
[30] C. Kittel, *Introduction to Solid State Physics*, 7th ed. (Wiley, New York, 1996).
[31] O. Moze, P. W. Mitchell, S. K. Burke, J. R. Davislld, and J. G. Booth, J. Phys. F: Met. Phys. **18**, 527 (1988).
[32] P. Söderlind, L. H. Yang, J. A. Moriarty, and J. M. Wills, Phys. Rev. B **61**, 2579 (2000).
[33] S. Han, L. A. Zepeda-Ruiz, G. J. Ackland, R. Car, and D. J. Srolovitz, Phys. Rev. B **66**, 220101(R) (2002).
[34] D. Nguyen-Manh, A. P. Horsfield, and S. L. Dudarev, Phys. Rev. B **73**, 020101(R) (2006).
[35] C. G. Shull and M. K. Wilkinson, Phys. Rev. **97**, 304 (1955).
[36] M. F. Collins and G. G. Low, Proc. Phys. Soc. London **86**, 535 (1965).
[37] A. T. Aldred, B. D. Rainford, J. S. Kouvel, and T. J. Hicks, Phys. Rev. B **14**, 228 (1976).
[38] H. W. King, Science **1**, 808 (1966).
[39] P. Olsson, I. A. Abrikosov, and J. Wallenius, Phys. Rev. B **73**, 104416 (2006).
[40] T. P. C. Klaver, R. Drautz, and M. W. Finnis, Phys. Rev. B **74**, 094435 (2006).
[41] A. Möslang, H. Graf, G. Balzer, E. Recknagel, A. Weidinger, Th. Wichert, and R. I. Grynszpan, Phys. Rev. B **27**, 2674 (1983).
[42] E. Kuramoto, S. Nagano, K. Nishi, K. Makii, Y. Aono, and M. Takenaka, Mater. Sci. Forum **105-110**, 1125 (1992).
[43] See EPAPS Document No. E-PRBMDO-75-054701 for a comparison of the Cr-defect interactions predicted by the USPP and PAW formalisms. For more information on EPAPS, see http://www.aip.org/pubservs/epasp.html.
[44] C. S. Becquart and C. Domain, Nucl. Instrum. Methods Phys. Res. B **202**, 44 (2003).
[45] R. A. Johnson, Phys. Rev. **134**, A1329 (1964).
[46] F. Maury, P. Lucasson, A. Lucasson, F. Faudot, and J. Bigot, J. Phys. F: Met. Phys. **17**, 1143 (1987).
[47] A. L. Nikolaev, V. L. Arbuzouv, and A. E. Davletshin, J. Phys.: Condens. Matter **9**, 4385 (1997).
[48] D. Terentyev, L. Malerba, and A. V. Barashev, Philos. Mag. Lett. **85**, 587 (2005).
[49] C. Domain and C. S. Becquart, Phys. Rev. B **71**, 214109 (2005).